AD-A116 356 BRISTOL UNIV (ENGLAND) F/G 11/9
GLASS FIBRE/EPOXY RESIN INTERFACE LIFE-TIME PREDICTION.(U)
MAR 82 K H ASHBEE, N R FARRAR, J P SARGENT DAJA37-81-C-0214
UNCLASSIFIED NL

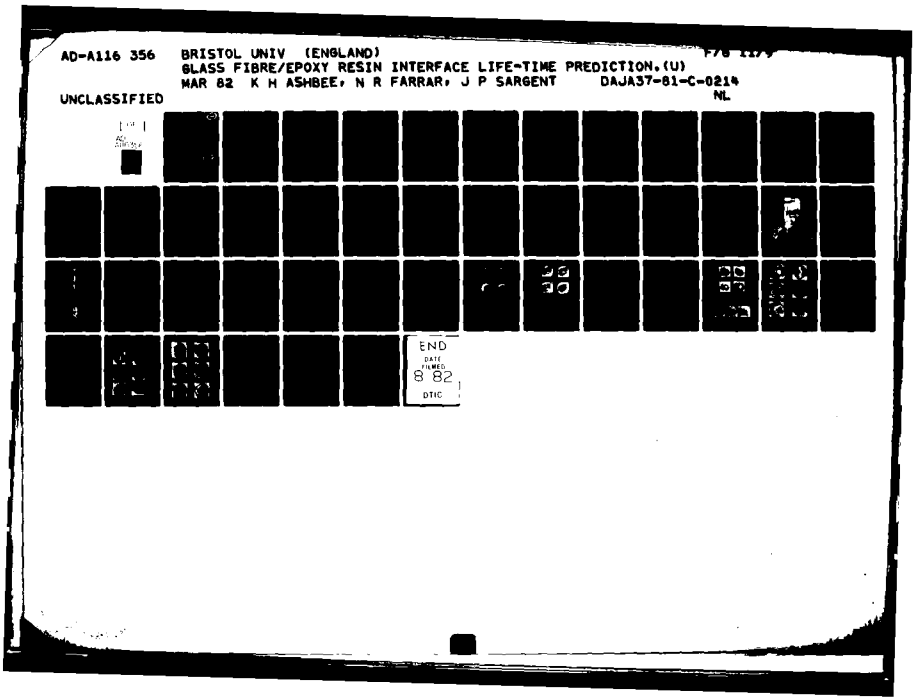

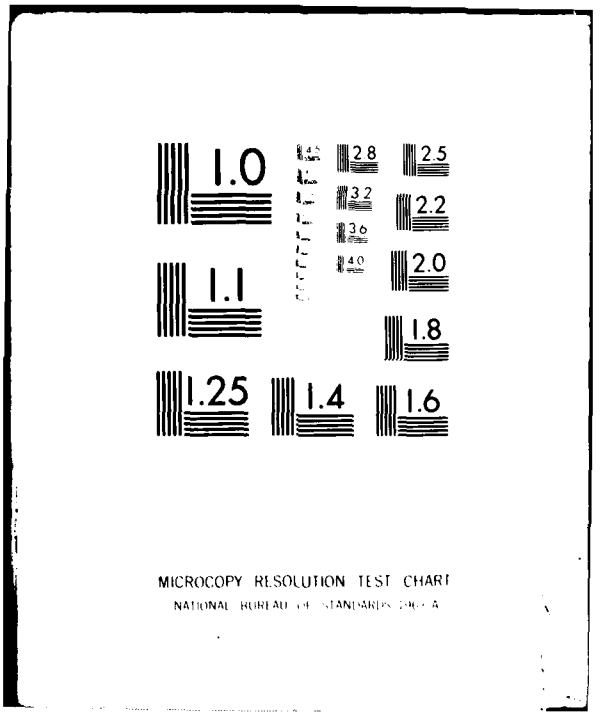
1.0
1.1
1.25
1.4
1.6
1.8
2.0
2.2
2.5
2.8
3.2
3.6
4.0
MICROCOPY RESOLUTION TEST CHART
NATIONAL BUREAU OF STANDARDS 1963-A

UNCLASSIFIED

SECURITY CLASSIFICATION OF THIS PAGE (When Data Entered)

REPORT DOCUMENTATION PAGE	READ INSTRUCTIONS BEFORE COMPLETING FORM
1. REPORT NUMBER / 2. GOVT ACCESSION NO. AD A116356	3. RECIPIENT'S CATALOG NUMBER
4. TITLE (and Subtitle) Glass Fibre/Epoxy Resin Interface Life-Time Prediction	5. TYPE OF REPORT & PERIOD COVERED Annual Technical Report March 1982
	6. PERFORMING ORG. REPORT NUMBER
7. AUTHOR(s) K.H.G. Ashbee, J.P. Sargent, N.R. Farrar, Elizabeth Walter	8. CONTRACT OR GRANT NUMBER(s) DAJA37-81-C-0214
9. PERFORMING ORGANIZATION NAME AND ADDRESS University of Bristol, Royal Fort, Tyndall Avenue, Bristol BS8 1TL, UK	10. PROGRAM ELEMENT, PROJECT, TASK AREA & WORK UNIT NUMBERS 1T161102BH57-04
11. CONTROLLING OFFICE NAME AND ADDRESS USARDSG-UK, Box 65, FPO NY 09510	12. REPORT DATE March 1982
	13. NUMBER OF PAGES 47
14. MONITORING AGENCY NAME & ADDRESS(if different from Controlling Office)	15. SECURITY CLASS. (of this report) Unclassified
	15a. DECLASSIFICATION/DOWNGRADING SCHEDULE

16. DISTRIBUTION STATEMENT (of this Report)

Approved for public release; Distribution unlimited

17. DISTRIBUTION STATEMENT (of the abstract entered in Block 20, if different from Report)

DTIC ELECTE JUN 30 1982 S D

18. SUPPLEMENTARY NOTES

19. KEY WORDS (Continue on reverse side if necessary and identify by block number)

Interfacial lifetime, Optical waveguide, Non Destructive Evaluation, Osmosis, Load transfer, Residual stress

20. ABSTRACT (Continue on reverse side if necessary and identify by block number)

The principle of fibre reinforcement requires load transfer from matrix to fibres. In resin matrix composites it is known, from measurements of mechanical strength, that realisation of load transfer is progressively impaired during water uptake from humid in-service environments. The physical mechanisms responsible for this impairement include the generation of interfacial pressure pockets, the occurrence of which suggests that the optical waveguide behaviour of glass reinforced plastics should be affected

DD FORM 1 JAN 73 1473 EDITION OF 1 NOV 65 IS OBSOLETE S/N 0102-LF-014-6601

UNCLASSIFIED

SECURITY CLASSIFICATION OF THIS PAGE (When Data Entered)

and might therefore offer a non destructive evaluation technique for monitoring at least one of the causes of mechanical degradation. This possibility has been appraised and experimentally verified.

Two models have been developed and applied to interfacial fracture at pressure pockets attributable to osmosis. Direct photoelastic measurements indicative of load transfer in short fibre composites have been used to test the rates of debonding predicted by the two models.

The net stress across the boundary of the first Wigner cell in a fibre reinforced composite must be zero from which it is inferred that, moving around a fibre, the radial principal stress changes sign several times. The origin of the stress can be differential thermal contraction between fibre and matrix materials during cooling from the resin cure temperature, or inhomogeneous swelling associated with water uptake, or externally applied loads. The number of reversals of sign is determined by the fibre lay-up geometry. In the light of this, interfacial failure is expected to initiate at sites located on the loci of maximum residual radial tension. Also, subsequent propagation of individual pressure pockets is expected to be favoured along these loci rather than around the fibre circumference. The fact that such preferred initiation and propagation are not observed is taken to mean that residual stress is more uniformly distributed than expected. The nature of residual stress generated during resin curing and during water uptake/expulsion has consequently been further investigated.

TABLE OF CONTENTS

LIST OF FIGURES

13. Part of a sequence of interference patterns photographed during the 30 minute cooling period for a glass slide/resin film (150μm thick) cover slip sandwich.

14. Moiré fringes (M) generated by superimposition of interference patterns (I) in order to reveal the deformation of the cover slip after quenching the cure temperature (135°C). The cover slip was 150μm thick.

15. Normal displacement across one diameter of the cover slip after 5 minutes at the cure temperature (135°C). (H_o=250μm)

16. Radial stress distribution for a cover slip subjected to buckling coefficients to produce the displacement shown in figure 15.

17. Moiré fringes generated by superimposition of interference patterns in order to reveal the deformation of the cover slip after quenching the cure temperature (135°C). The cover slip was 150μm thick.

18. Moiré fringes generated by superimposition of interference patterns in order to reveal the deformation of the cover slip during cooling down from the cure temperature to room temperature. The cover slip was 150μm thick.

19. (a) Plan of a succession of Moiré fringes taken during the UV water equilibration experiments. (b) Plan of a succession of Moiré fringes taken during rehydration experiments of the water absorbed in (a).

20. Displacement of a point (expressed as a percentage of the dry thickness) immediately adjacent to the edge of the specimen during several cycles of water uptake and expulsion.

21. (a) Moiré fringe formed between photographic images of points indicated as 1 and 2 in figure 2. (b) Moiré fringe formed between photographic images of points indicated as 3 and 4 in figure 2.

22. Comparisons of normalised photographic data of a saturated TGDDM specimen. (a) Immersed in deionised water at 23°C and (b) exposed to dry air at 23°C. This shows equivalence with effects of hygroscopy.

23. Comparisons of normalised photographic data of a TGDDM specimen immersed in deionised water at 40°C.

24. Graph of the progression of the hygroscopic edge of the cover slip specimen normalised as a function of time$^{1/2}$ for the experiments shown in figure 23.

25. Schematic diagram to illustrate the changing geometry of the corner edge during swelling of the adhesive in a joint exposed to an aqueous environment. Debonding follows saturation of swelling at the rim of the joint

26. Graph of the predicted water concentration $C(x,t)/C_0$ as a function of fractional distance from the middle of the specimen, x, points superimposed for different concentrations and positions corresponding to the debonding data shown in Figure 25. After Kinloch [ ].

2. [illegible]

[illegible]

$$\frac{\partial \rho}{\partial N} = [illegible]$$

$$\phi = [illegible]$$

$$\frac{\partial \rho}{\partial n} = [illegible]$$

$$\frac{\partial \rho}{\partial [illegible]} = [illegible]$$

[illegible]

$$[illegible]$$

[illegible]

$$[illegible]$$

[illegible]

[illegible]

2. [illegible]

2.1 [illegible]

[illegible]

2.2 Specimen preparation

For optical waveguides used in telecommunications, $(n_1 - n_2) \approx 10^{-2}$. The refractive index of fibreglass is close to 1.5 and, for applications where optical transparency is required - CRT windows for example - manufacturers try to match the refractive index of the cured resin to that of the fibreglass. They rarely succeed and, as often as not the refractive index mismatch is such that the waveguide condition is satisfied. The preparation procedure used to embed our unembedded composites manufactured by pressing epoxy resin into an evacuated split mould, was designed that it suppressed a controlled flow of fibres. A photograph of the mould is in Figure 2. A Mylar, plastic sheet with a 2mm hole drilled in the centre was sandwiched between the mould halves before clamping the mould closed. By varying the thickness and position of the sheet and by varying the depth of cuts, it is possible to embed a number of samples with different refractive indices of the matrix. For some specimens, the matrix was deliberately opaque by adding a blue pigment to the epoxy resin.

In principle, it should be possible to simultaneously measure the light via a light pipe with different angles of incidence, θ_0. However, in practice the specimen is not flat so the angle of incidence of the light on each part of the specimen surface will be different and the light is deflected by the birefringent fibres. The light source was a 5mW helium-neon gas laser which illuminated a 1mm diameter spot with light of wavelength 0.633μm. The light was measured using the Reflex mode of operation of the Talysurf 4 instrument. This instrument is normally used for measuring surface roughness. It has a very small angular aperture and is insensitive to light which has been scattered by the surface. Measurements of reflectance were made using the Talysurf 4 with the specimen mounted on a rotating table.

2.3 Experimental results and discussion

In order to check the experimental procedure, Snell's law was used to calculate the refractive index of a sample of Perspex from measurements of the critical angle. The refractive index was found to be 1.49 which is within the accepted range for Perspex. Measurements of reflectance were made on a number of specimens with different refractive indices. The results were found to be very sensitive to the angle of incidence of the light. Small changes in the angle of incidence caused large changes in the reflectance. Measurements of reflectance were made on specimens with different refractive indices. The results were found to be very sensitive to the angle of incidence of the light. Small changes in the angle of incidence caused large changes in the reflectance.

Polarising microscopy of very low fibre volume fraction specimens, Figure 4, reveals the occurrence of interfacial pressure pockets during the first 200 hours. During this time, the resin is also undergoing swelling in order to accommodate the diffused water, Figure 5. Before saturation, at around 200 hours, the concentration of diffused water and hence the swelling is inhomogeneously distributed and this, in turn, introduces compression near the external surface and tension deeper inside the composite. This stress field is superimposed on to that already generated by the differential thermal contraction between matrix and fibre materials during cooling from the resin cure temperature. The cumulative effect of these changing stresses is evidently discontinuous during the initial stages of water uptake.

Each pressure pocket is filled with aqueous solution and the critical angle over the area of contact between it and the fibre is larger than that for contact between resin and fibre. However, the expected propagation of a larger solid angle of light is not realised until coalescence of pressure pockets and release of elastic deformation is established along the whole length of the waveguide, i.e. not until a very much later stage of water uptake (~900 hours in figure 5).

5. [illegible] Hypothesis

5.1 Hypothesis

"In order clearly to explain the osmotic behaviour to be osmotic pressure, imagine a vessel, A (figure 6), completely full of an aqueous solution of sugar, placed in water, B. It must be conceived that the solid walls of this vessel are permeable to water, but impermeable to the dissolved sugar, which, owing to the attraction of the solution for water, water will enter the vessel A up to a certain limit, thereby increasing the pressure on the walls of the vessel. Equilibrium then ensues, owing to the pressure counteracting further entry of water. This pressure we have termed osmotic pressure." [illegible]

In this vessel A corresponds to interfacial pockets of water (of effective osmotic) which has diffused in from the outside environment and has dissolved water soluble species at the interface, vessel B corresponds to the [illegible] environment surrounding which the FRP composite resides, and the solid walls of vessel A thus are permeable to water but not to solute corresponding to the water soluble species. There is specific evidence for the occurrence of osmotically active pockets due to osmotic pressure first suggested by Scheirs and Verpoest [illegible] Examples of a resin/glass fibre/glass resin composite are shown in figure 7.

3.2 Model 1

When formed, each interfacial pocket closely resembles a penny-shaped crack that has grown in a solid tensioned between fixed grips. The overall change in energy is from U_0, corresponding to the state of strain energy prior to fracture, to $U_0 - U_G$, where the Griffith energy U_G given by the Zener approximation is

$$U_G = \frac{1}{2} \cdot \frac{2}{3} \cdot \frac{\sigma_1^2}{E} \pi a b^2 = \frac{\pi}{3E} \sigma_1^2 a b^2$$

$\sigma = \sigma_1$ is the tensile stress applied externally and perpendicular to the crack, E is Young's modulus, a and b respectively are the half thickness and radius of the crack. Referring to figure 8, if the interfacial cavity could be closed by application of traction on its wall, the stress σ_c [illegible] across the cavity would rise from σ to σ_1 and, correspondingly, its volume would decrease from V_1 to V_0.

The Griffith energy released by this process would be

$$U_G = \frac{1}{2} (\sigma_1 - \sigma_0)(V_1 - V_0) = \frac{\pi}{3E} (\sigma_1 - \sigma_0) a^3$$

Then

$$V_1 = \pi a^2 \cdot \frac{2}{3} a$$

In Model 1, [illegible] of the interfacial cavity varies with the external stress. The cavity is like a "balloon", i.e. it is full of internal pressure, and an external pressure $\sigma = \sigma_1$ gives the same V_1, see figure 9.

$$V_1 = \pi a^2 \cdot \frac{2}{3} a \cdot \frac{3}{4}$$

and the elastic strain energy is

$$U_{el} = \frac{1}{2} \sigma_1 V_1 = \frac{\pi}{4E} \sigma_1^2 a^3$$

Therefore $$\sigma_1 = \frac{2}{\pi a^2}$$

and $$U_{el} = \frac{\pi}{2E} \sigma_1^2 a^3$$

A solute exerts an osmotic pressure equal to the pressure that would be exerted by a gas having the same number of molecules in a volume equal to that occupied by the solution. Consider a change in volume of the interfacial cavity from V_o to V_1 resulting from dissolution of n moles of solute.

$$pV = nRT$$

The strain energy release = $\int pdV$

$$= \int_V nRT \; dV$$

$$= nRT \log_e \frac{(V_o + V_1)}{V_o}$$

$$= nRT \log_e \frac{p_1}{p_o}$$

p_o and p are the values of the osmotic pressure corresponding to volumes V_o and V_1 respectively.

The overall energy $E = E_{gas} + E_{elastic}$

$$= -nRT \log_e \frac{(V_o + V_1)}{V_o} + \frac{3}{8\pi} \frac{E V_1^2}{ab^3}$$

This function is sketched in Figure 10.

The value of V_1 corresponding to minimum energy release may be found by differentiation

$$\frac{dE}{dV_1} = -nRT \frac{1}{V_o + V_1} + \frac{3}{4\pi} \frac{V_1}{ab^2}$$

$$= 0 \text{ when } V_1^2 + V_1 V_o - \frac{4\pi}{3} ab^2 nRT = 0$$

i.e. when $V_1 = -\frac{V_o}{2} + \sqrt{\frac{V_o^2}{4} + \frac{4\pi ab^2 nRT}{3}}$

We must take the positive root, hence

$$V_1 = -\frac{V_o}{2} + \sqrt{\frac{4ab^2nRT}{3E}\left(1 + \frac{3EV_o^2}{16\pi ab^2 nRT}\right)}$$

$$\sim -\frac{V_o}{2} + \sqrt{\frac{4ab^2nRT}{3E}} \qquad \text{for large values of } b$$

3.3 Model 2

Alternatively, interfacial failure due to cracks inflated by osmotic pressure could be modelled as follows. Suppose a constant pressure reservoir supplies the "gas"

$$\text{Energy, } E = -p_1 V_1 + \frac{1}{2}p_1 V_1 = -\frac{1}{2}p_1 V_1$$

$$= -E_{elastic} = -\frac{2\pi}{3}\frac{p_1}{E}^2 ab^2$$

but $E_{surface} \sim 2\gamma\ \pi\ ab$, where γ is the specific surface energy

$$\text{so } E_{total} = 2\gamma\ \pi\ ab - \frac{2\pi}{3}\frac{p_1}{E}^2 ab^2$$

$$\frac{\partial E}{\partial b}_{total} = 2\gamma\pi a - \frac{4\pi}{3}\frac{p_1}{E}^2 ab$$

$$= 2\pi a\left(\gamma - \frac{2}{3}\frac{p_1}{E}^2 b\right)$$

which is negative if

$$b > \frac{3E\gamma}{2p_1}2 \qquad \text{i.e. if } p > \sqrt{\frac{3E\gamma}{2b}}$$

$$\frac{\partial E}{\partial a}_{total} = 2\gamma\pi b - \frac{2\pi}{3}\frac{p_1^2}{E} b^2 = 2\pi b\left(\gamma - \frac{p_1^2}{3E} b\right)$$

and is negative if $b > \frac{3E\gamma}{p^2}$

$\frac{\partial E}{\partial b}_{total}$ is evidently more negative than $\frac{\partial E}{\partial a}_{total}$, so the expression for p_{crit} is taken from the former.
Taking as trial values E = 3GPa, γ = 1J/m^2 and b = 10μm,

$$p_{crit} = \sqrt{\frac{3.3\times10^{9}.1}{2 \quad 10^{-5}}} = 10\text{MPa}$$

3.4 Observations

It is important to note the distinctive behaviour of pressure filled interfacial cracks under the two extreme types of inflation outlined in models 1 and 2. Model 2 corresponds to the uniform tensile stress type of loading that was treated by Griffith, and gives rise to an unstable critical crack size such that a smaller crack will not grow while a larger one will grow without limit. This critical crack size corresponds to a maximum in the sum of mechanical and surface energies. Model 1 implies loading at the mouth of the interfacial crack (as by the driving in of a wedge) and results in a stable crack size corresponding to a minimum in the sum of mechanical and gas energies.

Thus, model 2 predicts instantaneous interfacial failure if a constant osmotic pressure equal to a critical pressure can be maintained, whereas model 1 predicts interfacial failure at a rate determined by the requirement that each pressure pocket maintains its volume at a minimum energy level.

In Figure 11, the overall rate of interfacial failure is taken as the rate of loss of load transfer index in short fibre composites. The load transfer index is the optical retardation measured through diameters close to the centre of an individual short fibre minus the optical retardation measured through diameters near the ends of the same fibre. It is evident that interfacial failure proceeds at a rapidly decelerating rate such as would be expected if model 2 dominates at the time of initiation but gives way to model 1 during propagation.

According to model 1, interfacial pressure pockets maintain their volumes at values determined by the square root of the number of moles of dissolved solute. It has been observed that solutes can be leached from the fibre in some cases[4], leaving an 'etched' fibre surface, and in such cases the availability of the solute is presumably governed by the rate of diffusion of the solute to the surface of the fibre. The simplest diffusion model predicts dependence on the square root of time, and the combination of these two processes leads to a dependence of the volume of the interfacial pressure-filled cavities on the fourth root of time. The broken line in Figure 11 corresponds to a $(\text{time})^{1/4}$ law.

4. ON THE ASSUMPTION THAT EPOXY RESINS ARE FREE FROM SHEAR STRESS DURING CURE

4.1 Hypothesis

The accelerated cure reactions that take place during the elevated temperature curing of epoxy resins promote cross-linking and thereby give rise to shrinkage. There are no superimposed dimensional changes attributable to such processes as chain scissioning, as could be the case in polyesters that contain diffused water, or to the release of volatiles, as might be the consequence of condensation reactions in polyamides for example. The shrinkage is assumed to be homogeneous because any tendency to create shear stress is thought to be relieved by viscoelastic flow. This assumption is based on the premise that before it gels, the fluid resin behaves in a Newtonian fashion and is unable to support shear stress.

4.2 Experimental

19mm diameter soda-lime glass cover slips of two different thicknesses were bonded to 1mm thick soda-lime glass microscope slides. The cover slip thicknesses were 140μm and 230μm respectively and, the epoxy adhesive was Redux 312/5. The cover slips and microscope slides were thoroughly cleaned by ion bombardment before manufacturing the joints. Each specimen was mounted in a specimen chamber so that the free surface of the cover slip was in close proximity to an optical flat. This assembly was then mounted on an optical bench. In order that a uniform temperature distribution was maintained across the specimen, it was mounted on a thick disc of copper. This in turn was held in good thermal contact with the aluminium specimen chamber. Figure 12 is a schematic diagram of the optical components. The space between cover slip and optical flat is made small enough to allow optical interference between light incident upon and reflected from the free surface of the cover slip. Any changes in shape of the interference cavity, due to deformation of the cover slip caused by non-uniform changes in dimensions of the epoxy layer, cause the pattern of interference fringes to change.

Figure 13 shows a sequence of interference photographs recorded during the warm up period of a specimen manufactured with a 140μm thick cover slip. The time taken for the specimen to reach the cure temperature was 30 minutes and a substantial amount of the shape change occurred during this heating-up period. Initially, the cover slip is slightly deformed convex upwards but this soon gives way to a much larger concave deformation, the subsequent development of which is further examined in Figure 14 by creating Moiré patterns between successive photographs of the interference pattern and the pattern photographed when the specimen had completed its half hour cure. The Moiré fringes are the circumferential fringes, each

of which is the locus of points that have suffered identical displacement normal to the joint. The normal displacement of adjacent loci differ by half a wavelength.

4.3 Results and Discussion

Figure 15 shows the normal displacement at different points across a diameter of the same specimen after 5 minutes at the cure temperature, where t_o = 30 minutes is the total time at the cure temperature. The sign of the displacement field was established by applying an identical positive pressure to the cover slip. The curve fits the parabola

$$w = .071 \quad (x - .0095)^2$$

where w is the normal displacement and x is the distance measured from the edge of the specimen

To a first approximation, the deformation of the cover slip can be regarded as identical to that of a circular membrane, rigidly supported at its edge and subjected to a pressure drop (p) across its surfaces. For such a membrane, Love[5] has shown that the fourth differential of the normal displacement is a measure of p. The cover slip is thin. If thin enough for Love's analysis to be applied, then

$$\nabla^4 w = 0 \text{ when } p = 0$$

Since the data presented in Figure 15 is described by a parabola, the fourth differential $\partial^4 w/\partial x^4$ and hence the normal stress σ_{zz} are evidently zero.

Hence it is concluded that the deformation presented in Figure 15 is caused by radial stresses transmitted from the resin to the cover slip and not the stresses created normal to the joint. To check that curing really does cause the parallel sided disc of resin to transform into a concave lens shape, a specimen was manufactured using cover slips for both adherends. As expected, curing caused this sandwich to deform into a double concave lens as might have been produced by the application of edge tractions.

The analogy to the buckling of a thin circular plate simply supported around its edge and subjected to a uniformly distributed edge force applied in the plane of the plate, has been used to estimate the radial stress in the specimen shown in Figure 13.

The relations between the strains, displacements and stresses as given by Stoker[6] are

$$\varepsilon_{xx} = \frac{\partial u}{\partial x} + \frac{1}{2}\left(\frac{\partial w}{\partial x}\right)^2 = \frac{1}{E}(\sigma_{xx} - \nu\sigma_{yy})$$

$$\varepsilon_{xy} = \frac{1}{2}\left(\frac{\partial u}{\partial y} + \frac{\partial v}{\partial x} + \frac{\partial w}{\partial x}\frac{\partial w}{\partial y}\right) = \frac{1}{E}(1+\nu)\sigma_{xy}$$

$$\varepsilon_{yy} = \frac{\partial v}{\partial y} + \frac{1}{2}\left(\frac{\partial w}{\partial y}\right)^2 = \frac{1}{E}(\sigma_{yy} - \nu\sigma_{xx})$$

where the u,v,w components of the displacement of a point on the middle surface of the plate are denoted by u,v,w respectively.

The middle surface stresses divided by the modulus of elasticity E are denoted by σ_{xx}, σ_{xy}, σ_{yy} and the middle surface strains by ε_{xx}, ε_{xy}, ε_{yy}.

Since we assume radial symmetry, we may put $\sigma_{xx} = \sigma_{yy}$ and making the approximation that $\frac{\partial u}{\partial x}$ is sufficiently small relative to $\frac{1}{2}\left(\frac{\partial w}{\partial x}\right)^2$ such that it may be neglected gives

$$\frac{1}{2}\left(\frac{\partial w}{\partial x}\right)^2 = \sigma_{xx}(\nu - 1)$$

where ν = Poisson's ratio

Figure 16 shows the distribution of stress $\sigma_{xx} = f(r)$ obtained using the above equation for the deformation shown in Figure 15.

The above estimate is based on a deformation which is wholly elastic. An alternative estimate, using a simple viscoelastic model, is as follows. The raw adhesive film has a larger thermal expansion coefficient than glass. During heating to the cure temperature, the resin is free to expand in the thickness direction but radially it has to work against viscosity and its velocity relative to the glass is zero or close to zero at contact, becoming progressively larger at deeper layers. As a consequence, the cover slip is deformed convex upwards. Approaching the cure temperature, the shrinkage associated with the accelerated cure reaction dominates and the cover slip deformation is reversed to the concave shape sketched in Figure 15. An order of magnitude estimate of the in-plane shear stresses is obtained as follows. The adhesive layer is 150μm thick and 19mm in diameter, so the ratio of unrestricted in-plane shrinkage to thickness shrinkage is

$$= 150 \times 10^{-6}/9.5 \times 10^{-3} = 1.58 \times 10^{-2}$$

Because the [illegible] cells move from the plane surface in of the order $1.3 \times 10^{-7} \times 4 \times 10^{-6}$ m. Most of this outdistance occurs during the first few minutes of temperature, during which time the average shrinkage strain may [illegible] be approximately $5 \times 10^{-3}/30.5 \times 10^{-3} \times 5 \times 60\ sec^{-1} \times 1.6 \times 10^{-6}\ sec^{-1}$. Whilst still a liquid, and hence it becomes a gel, the viscosity (η) of the resin is probably in the range 1-10 Pas.

Hence the stress $\sigma = \eta \dot{\varepsilon}$

$$= 1.6 \times 10^{-7} \text{ to } 1.6 \times 10^{-6}$$

The true magnitude of the hoop-line stress presumably lies somewhere between that for the wholly elastic and that for the wholly viscoelastic estimate. Hence it is concluded that, even at the cure temperature, a thin layer of epoxy during thermosetting typical of the spacing between fibres in a composite shows induced enough measurable shear stresses.

Figure 17 shows a sequence of Moiré patterns during a 120C cure of a specimen manufactured with a 7.5μm thick coated slip. A perceptible deformation is established similar to that obtained for the specimen in Figure 11 but of smaller magnitude.

Figure 18 shows a sequence of Moiré patterns for the specimen from Figure 16 on cooling from the cure temperature. In addition to a small increase in the inverse deformation during cooling (when the fibres presumably behave as an elastic medium with contraction of the resin resembling that in the glass cured state), the Moiré patterns reveal a potentially complex deformation, as shown by small loops and contortions on the circumferential fringes. These may be associated with local inhomogeneities such as air bubbles.

3. THE IRREVERSIBILITY OF DIMENSIONAL CHANGES IN EPOXY RESINS UNDERGOING UPTAKE AND EXPULSION OF WATER

3.1 [illegible]

Earlier experiments suggest that the accommodation of water in epoxy resins and the consequences of this accommodation are reversible. Thus the increase in weight during water uptake can be more or less reversed by drying [illegible] as can the associated change in glass transition temperature[illegible]. The information sought in the experiments reported in this section relates to the dimensional stability of resins during the uptake and expulsion of [illegible] water and is, therefore, more fundamental to an understanding of the apparent reversibility of accommodation of water.

3.2 Method

See Section 2.2.

3.3 Results

Figure 13(a) is a sequence of Moiré images obtained for a specimen manufactured from [illegible] epoxy adhesive [illegible] and formed by [illegible] on [illegible] the photograph taken at time t = 0, corresponding to the commencement of water uptake. Figure 13(b) is another sequence taken during subsequent expulsion of this water, [illegible] and the "base line" photograph for the [illegible] sequence was that taken at [illegible], i.e. that corresponding to the commencement of water expulsion. Figure [illegible] is a plot of the displacement of a point immediately adjacent to the edge of the specimen over several cycles of water uptake and expulsion.

Comparison of Moiré patterns from images photographed at identical moments of swelling, and which are separated by one or more water uptake/expulsion cycles, permits immediate detection of any irreversible changes in the adhesive film dimensions. Figure 15(a) is a Moiré pattern formed between photographs taken at the points designated as X and X' in Figure 14 (representing states of maximum water uptake). Figure 15(b) is another pattern corresponding to Y and Y' in Figure 14 (representing states of minimum water uptake). Although the absence of any substantial Moiré patterns in either of the figures 15(a) or 15(b) indicates that repeated cycling has on the whole led to only a limited irreversible change in the displacement field, small changes are evident. One such change is indicated by an arrow in Figure 15(b) and shows the appearance of small Moiré loop indicating that a permanent irreversible local swelling displacement has occurred.

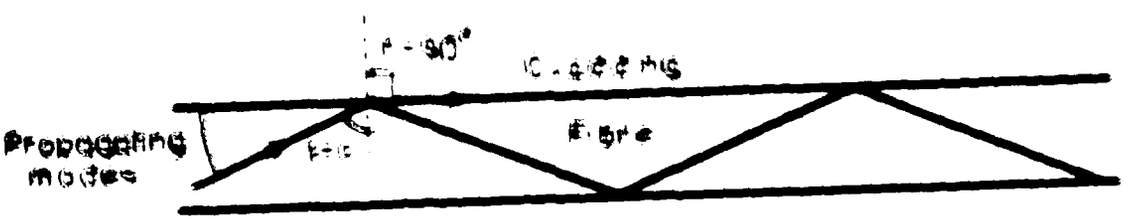
Propagating
modes

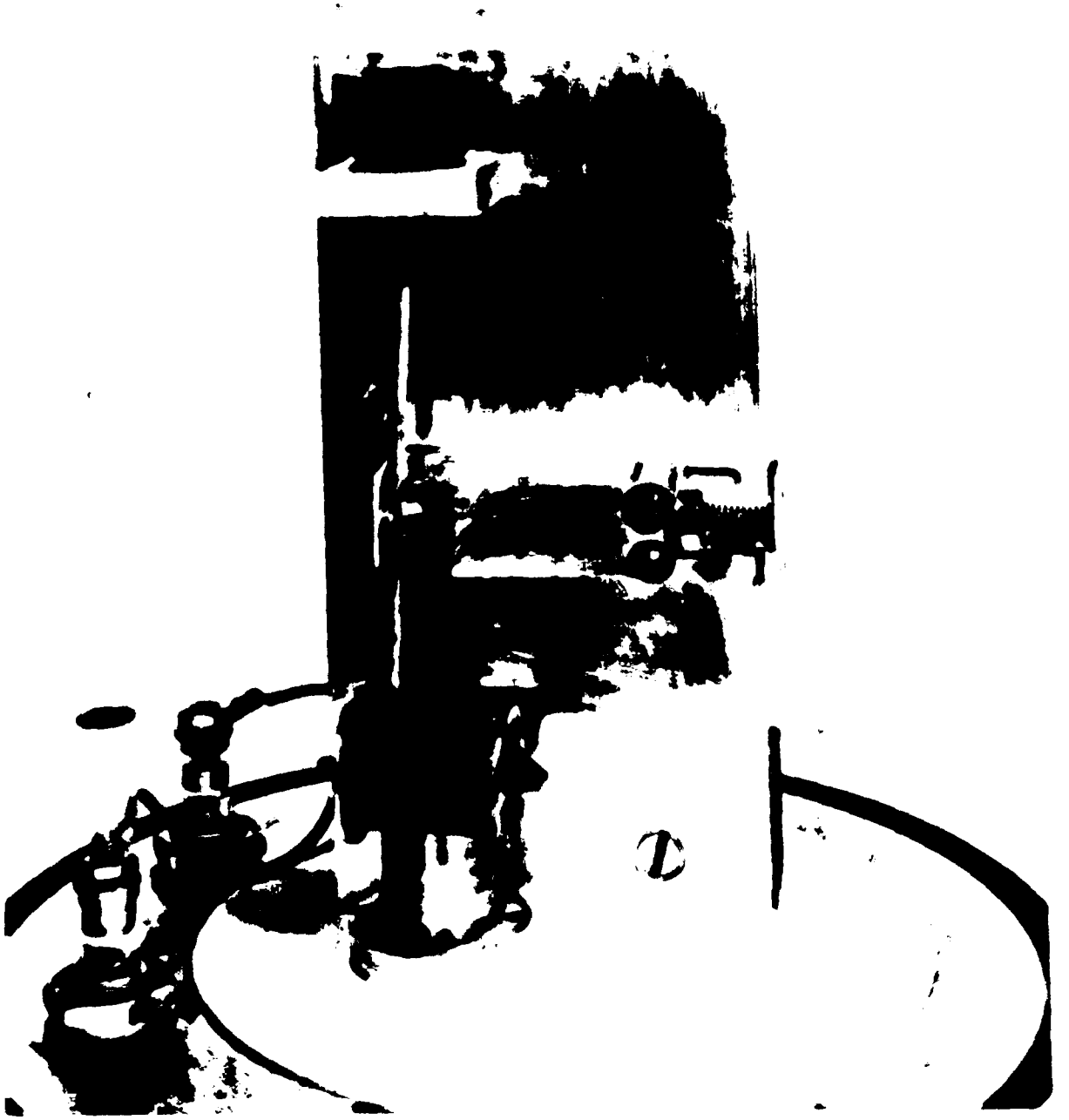

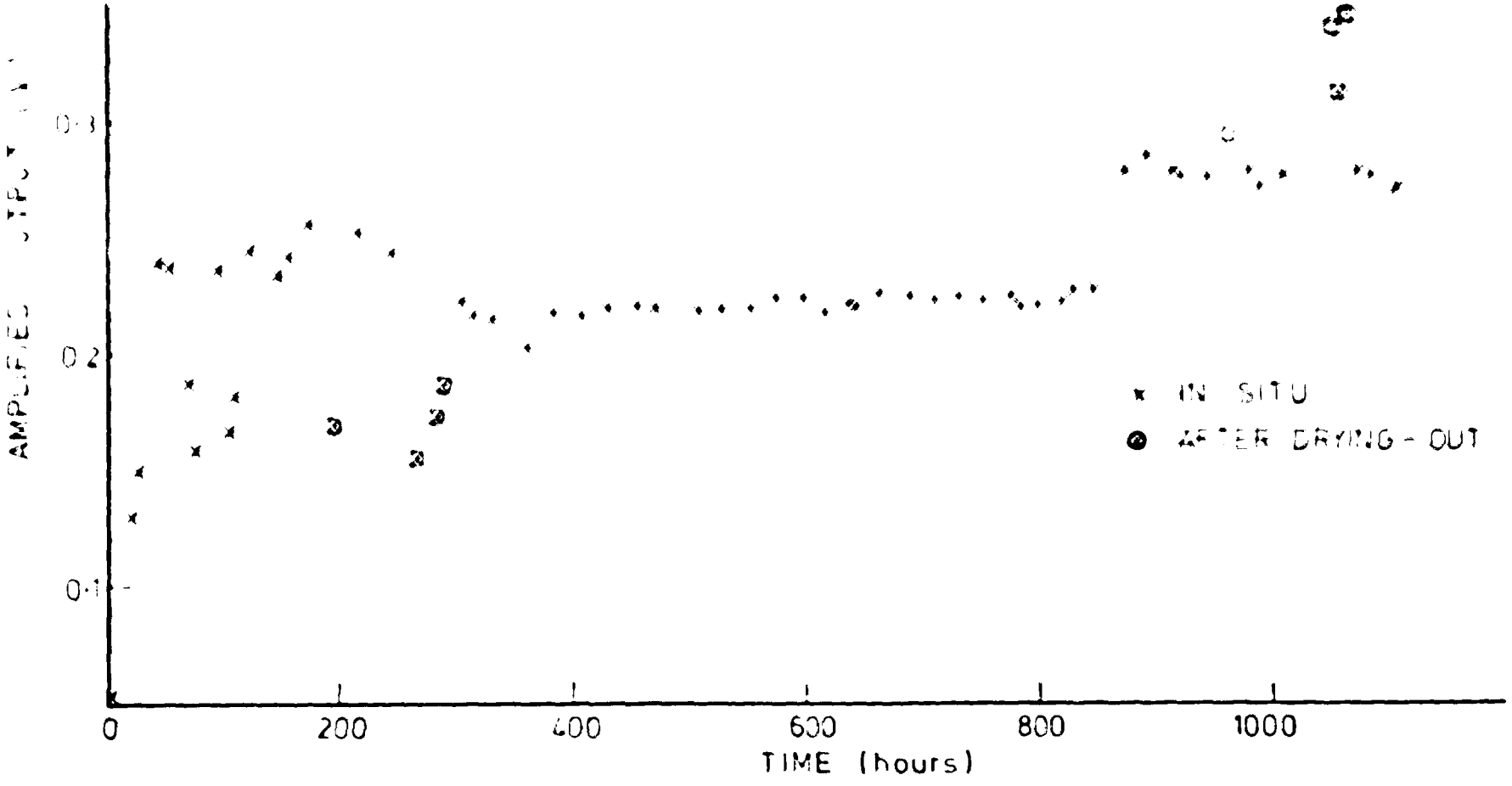

3. Optical waveguide test on GRP. Tow of 10μm diameter E-glass fibres in epoxy resin. $V_f = 43.2\%$. Coupon immersed in distilled water at

[redacted]

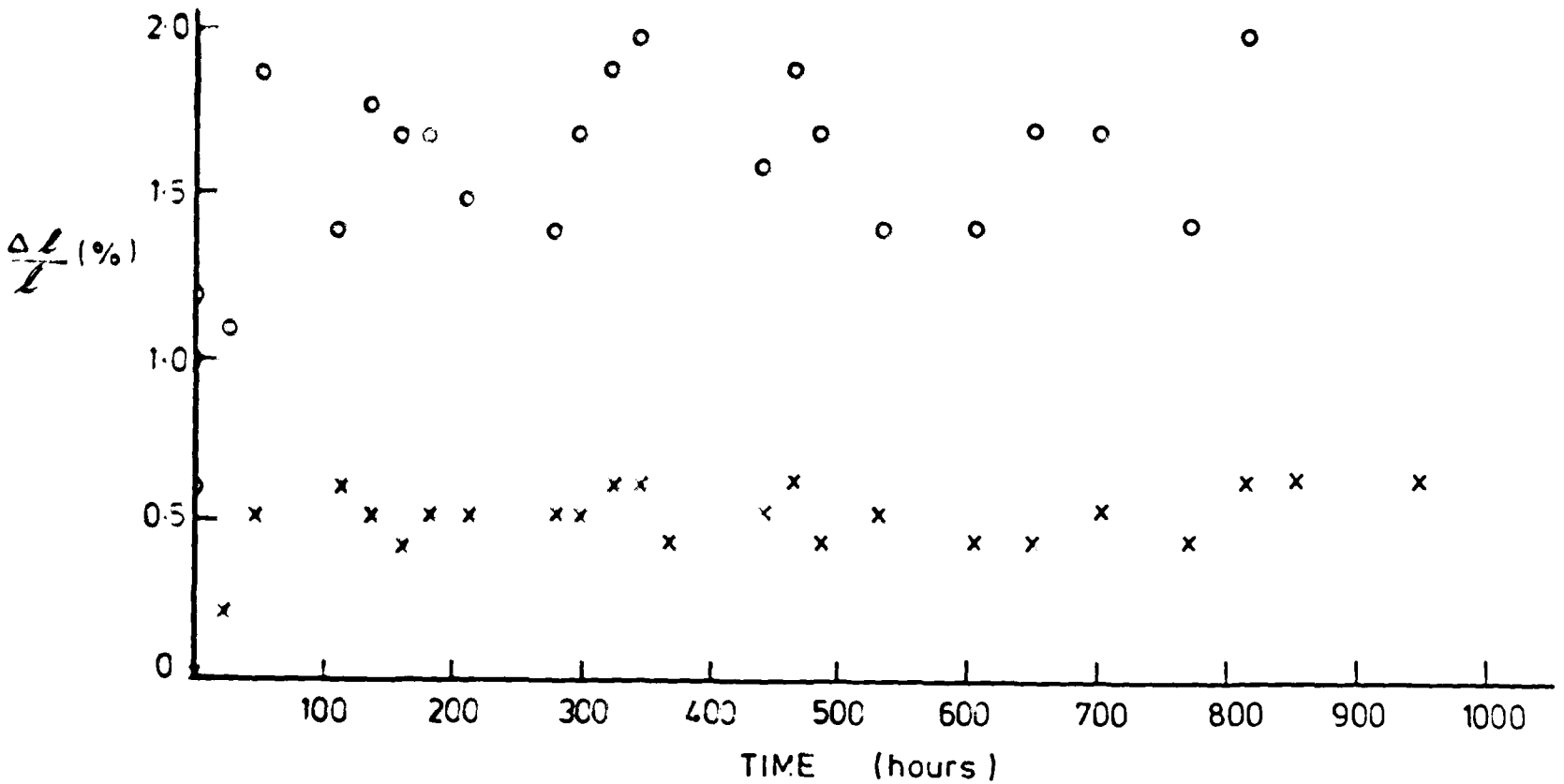

5. Change in linear dimensions during swelling associated with water uptake at 100°C by two epoxy resin slabs

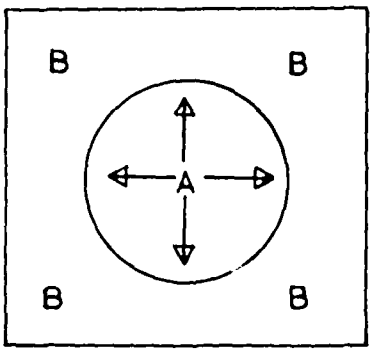

6. After van't Hoff (1888)[3]

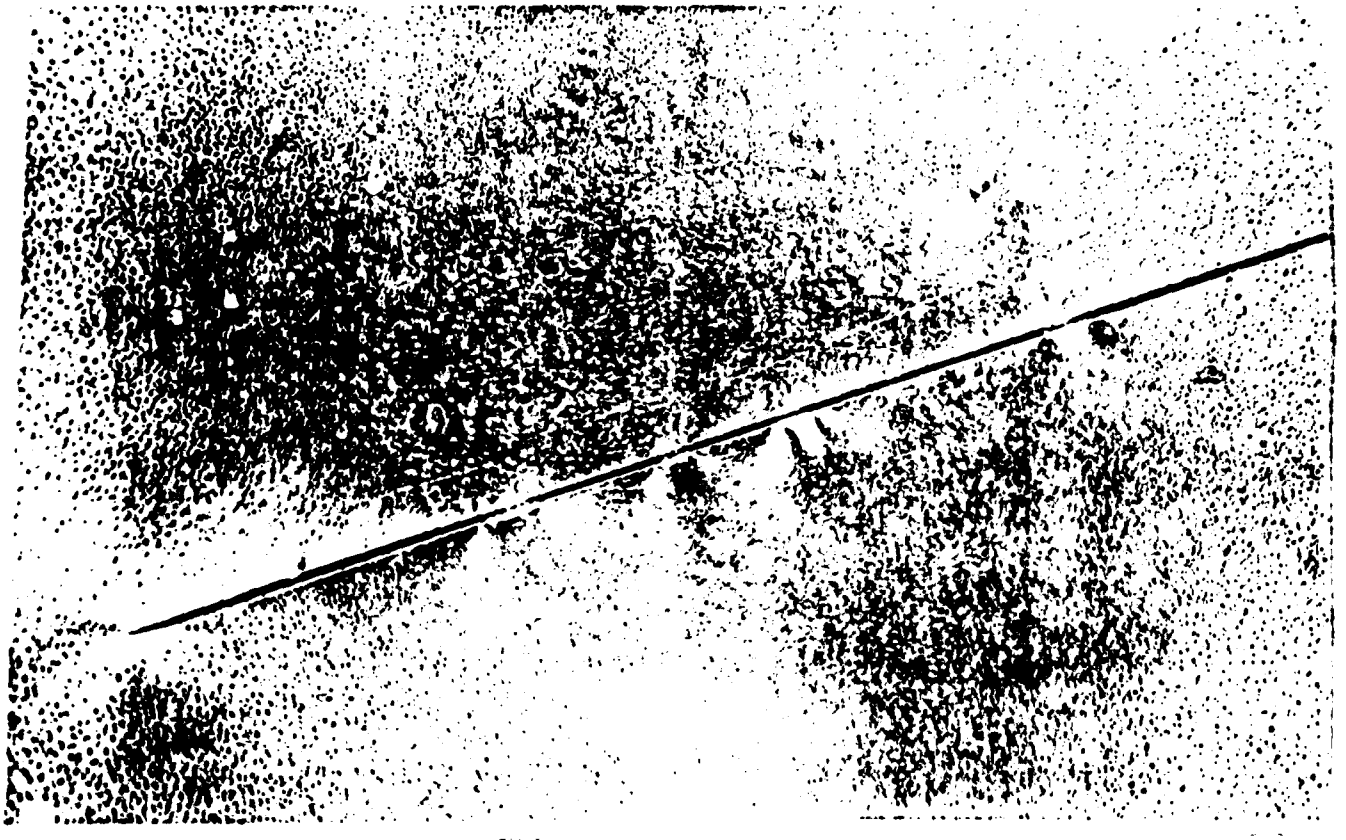

7. Photoelastic contrast caused by pressure pockets on the surface of a graphite fibre in an epoxy matrix composite after 600 hrs immersion in distilled water at 80C

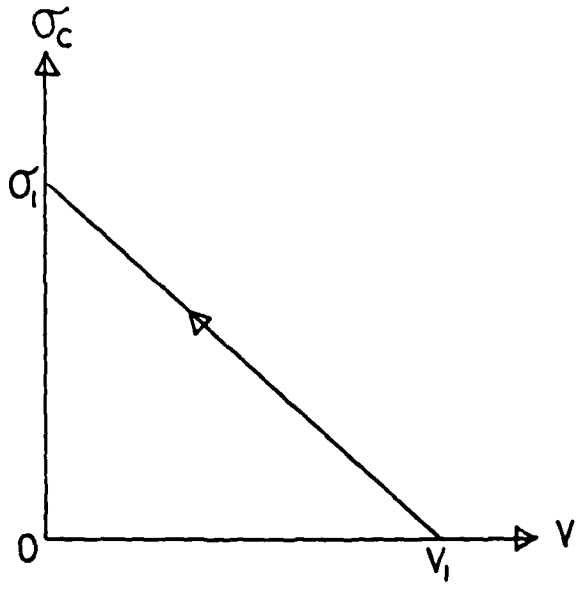

8. Applied stress as a function of volume of a Griffith's crack

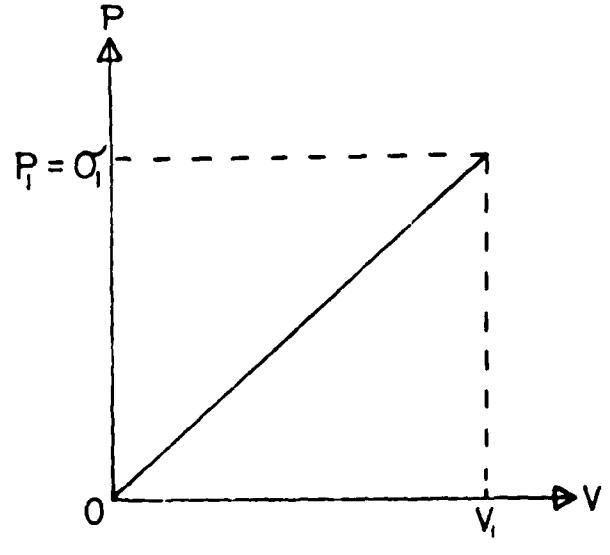

9. Crack volume versus internal pressure for an inflated crack

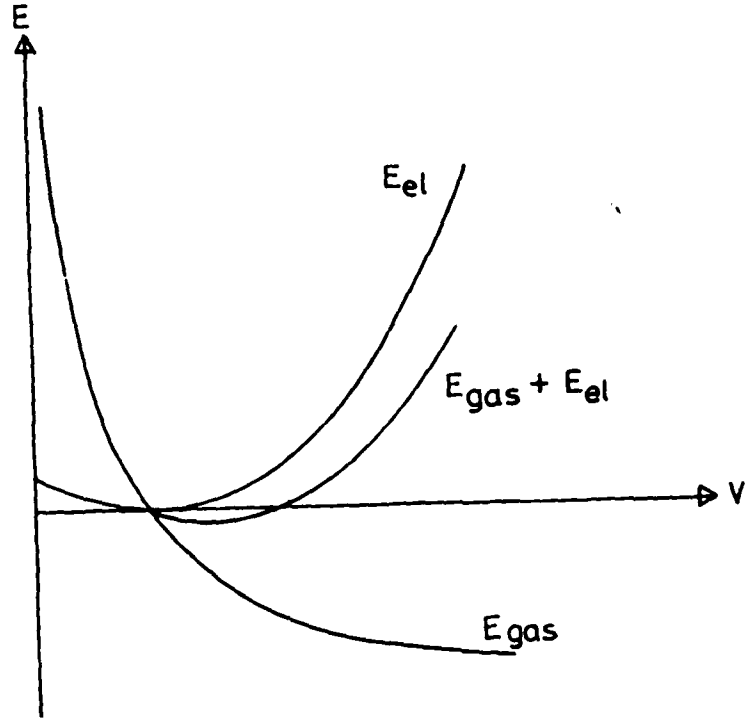

10. Energy versus volume of an inflated crack

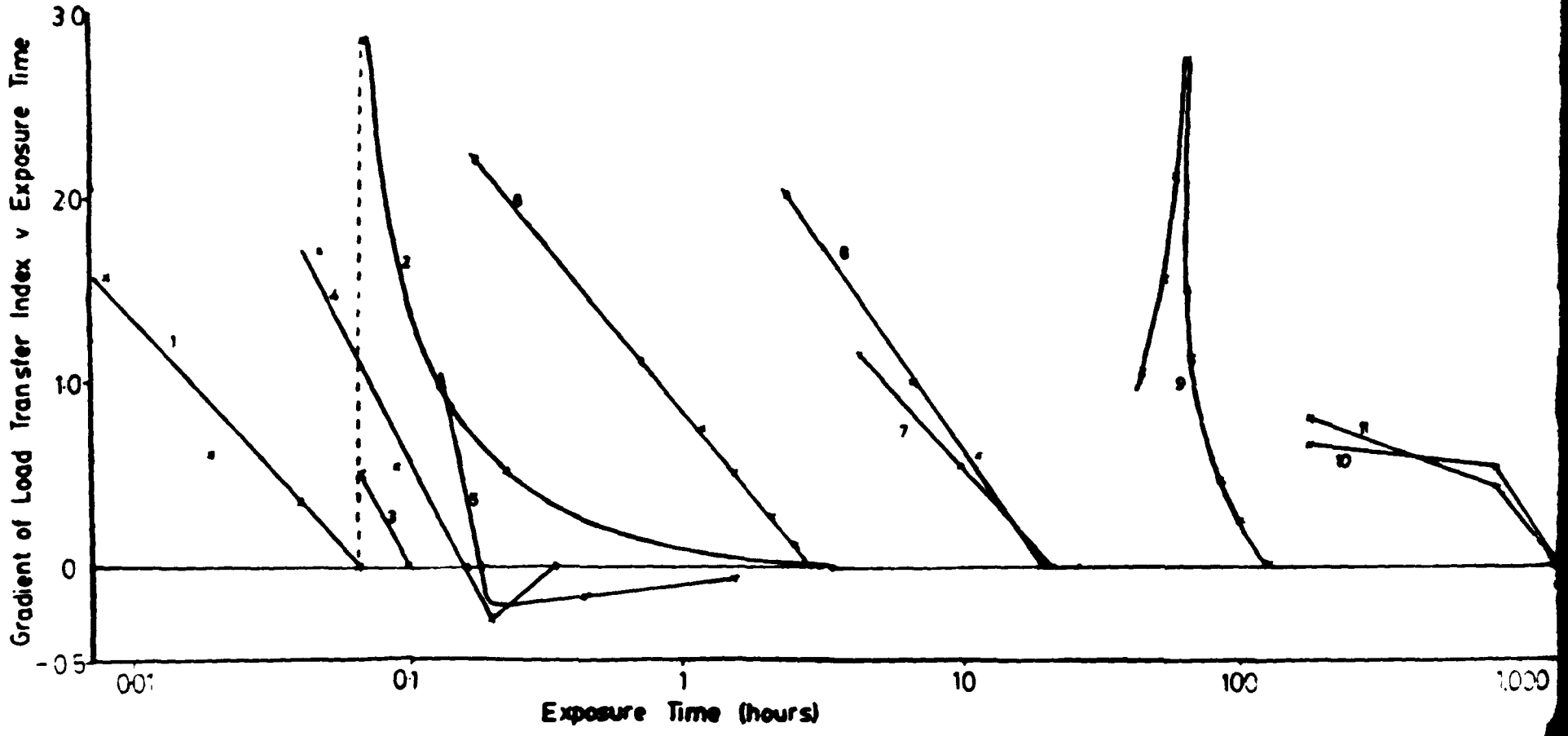

11. Rate of loss of load transfer index during water uptake by various resin matrix composites.
    (1) E-glass/polyester 100C
    (2) Second immersion of specimen 1 after drying 100C
    (3) E-glass (no coupling agent) polyester 100C
    (4) E-glass (no coupling agent) polyester 100C
    (5) E-glass/polyester 100C
    (6) E-glass/polyester 20C
    (7) E-glass/polyester 20C
    (8) E-glass/epoxy 100C
    (9) E-glass/polyester 100C
    (10) S-glass/epoxy 80C
    (11) S-glass/epoxy 80C

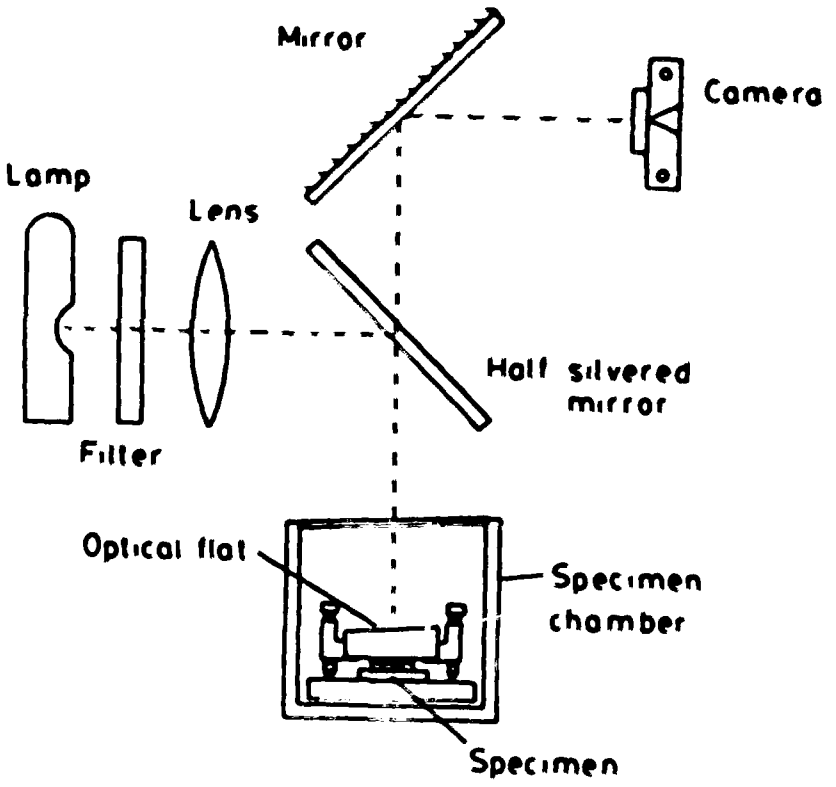

12. Schematic representation of the optical bench used for optical interference studies of dimensional stability of resins

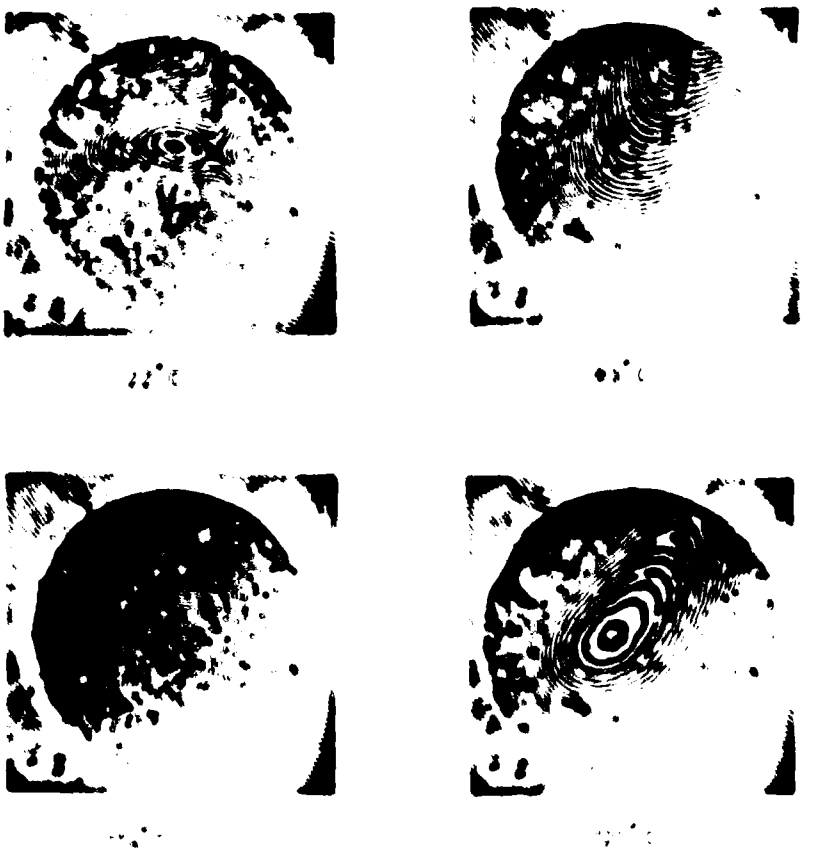

13. Part of a sequence of interference patterns photographed during the 10 minute warming period for a glass slide/resin film/[illegible] thick cover slip sandwich

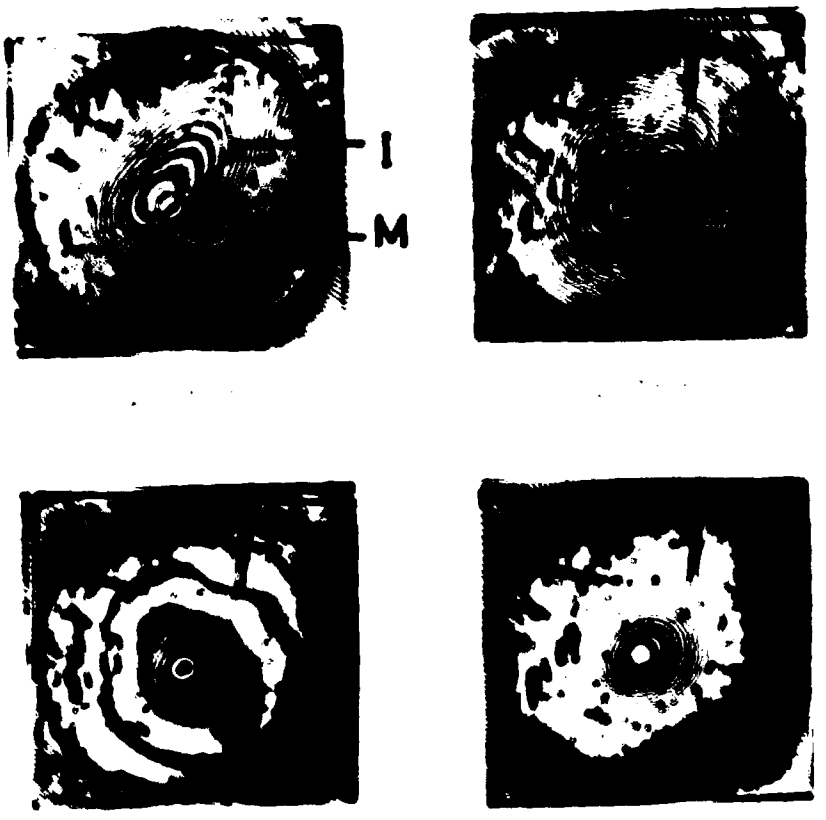

Fig. Mixed [illegible] ... [illegible] ... patterns ... [illegible] ... about ... [illegible] ... phase.

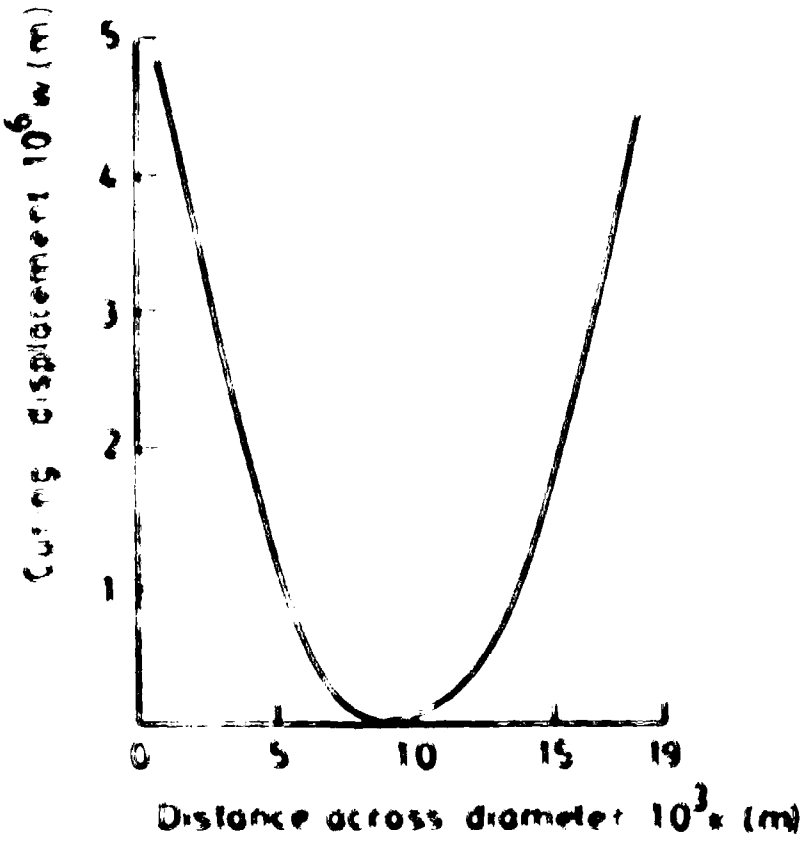
5
4
3
2
1
0
5
10
15
19
Distance across diameter $10^3 x$ (m)

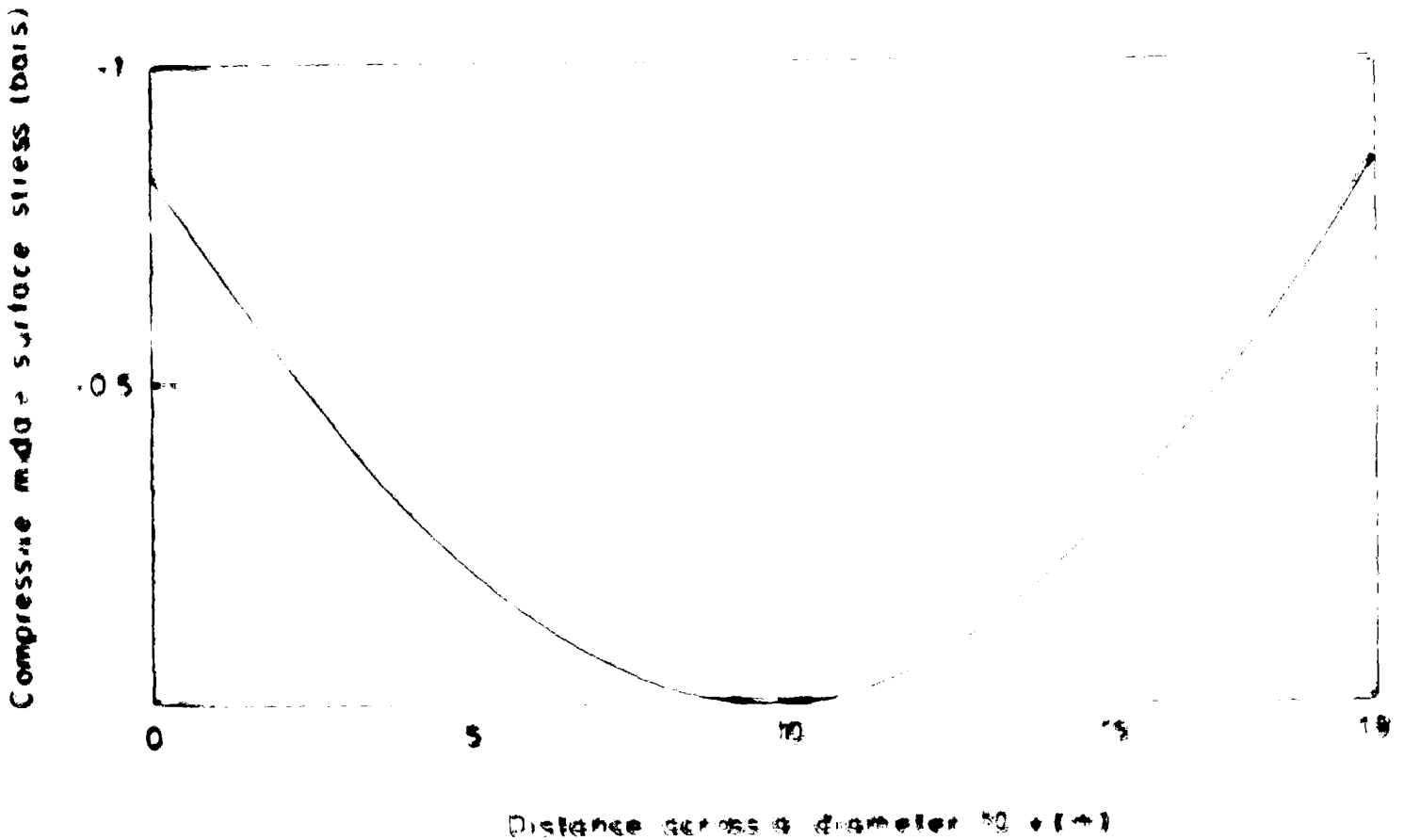
Compressive mean surface stress (bars)
-1
-.5
0
5
10
15
19
Distance across diameter (mm)

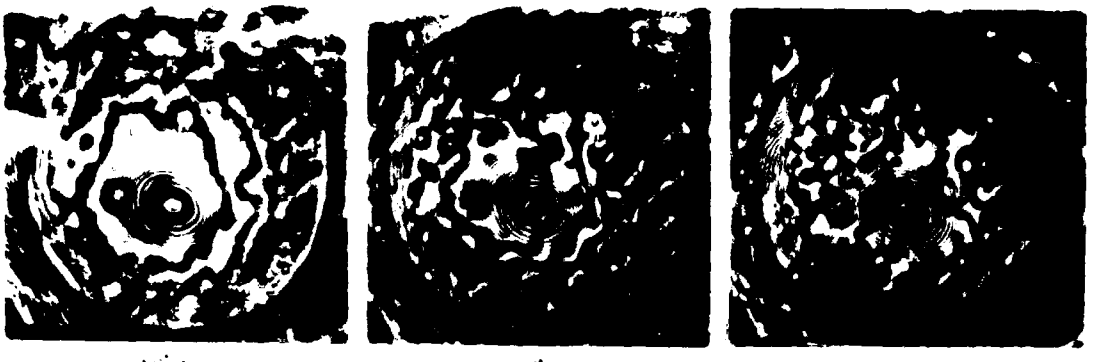

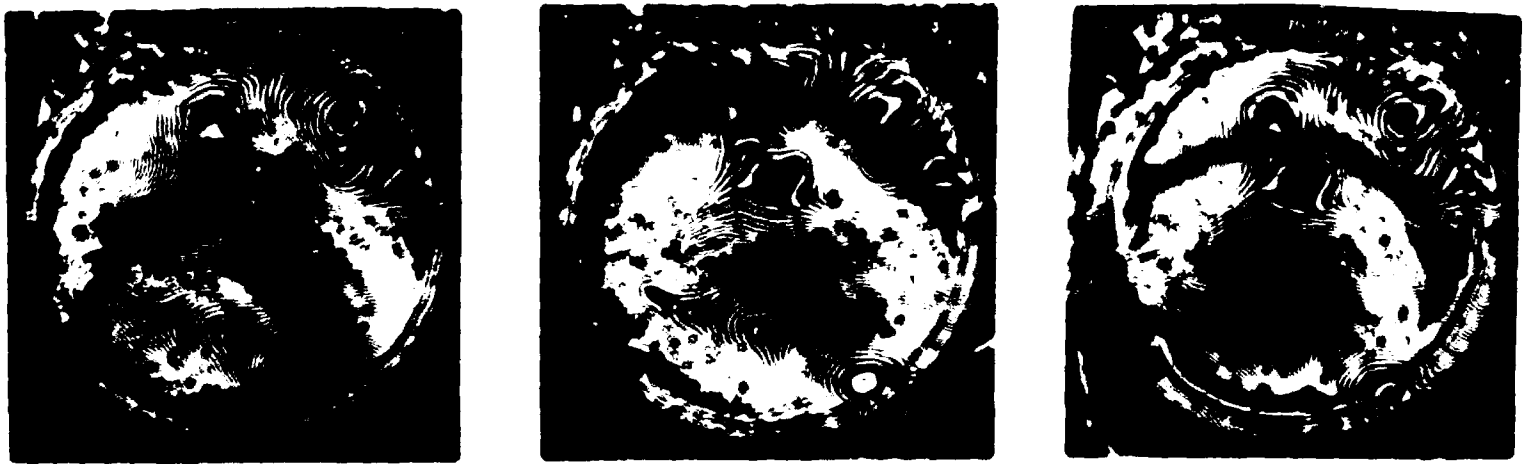

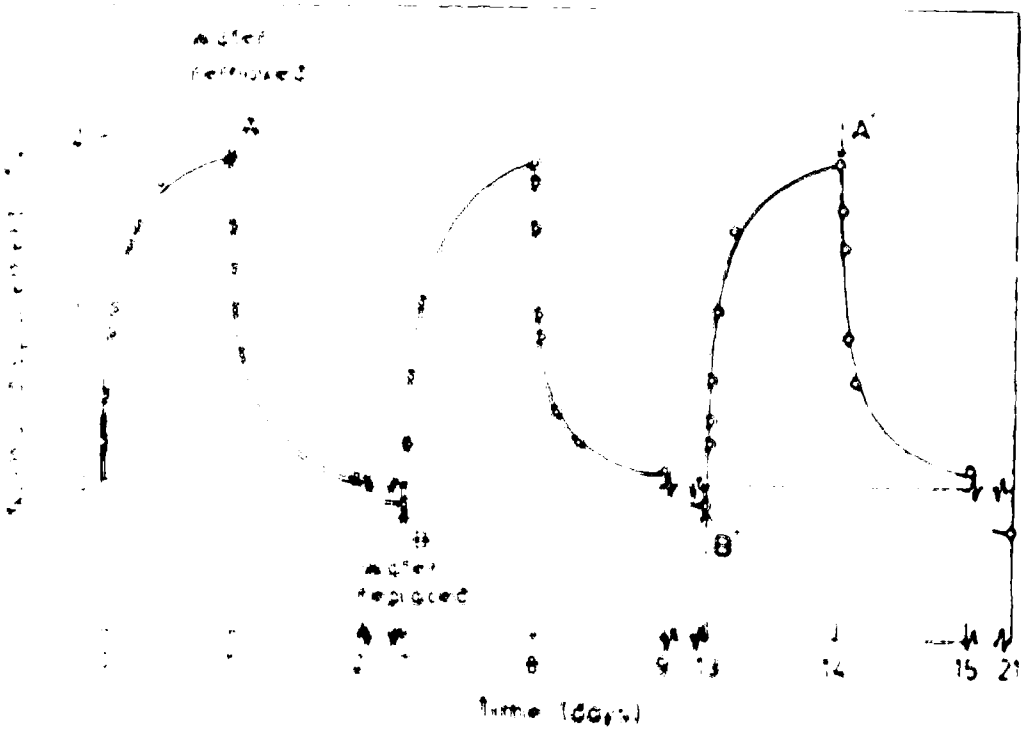
A'
B'
15
21

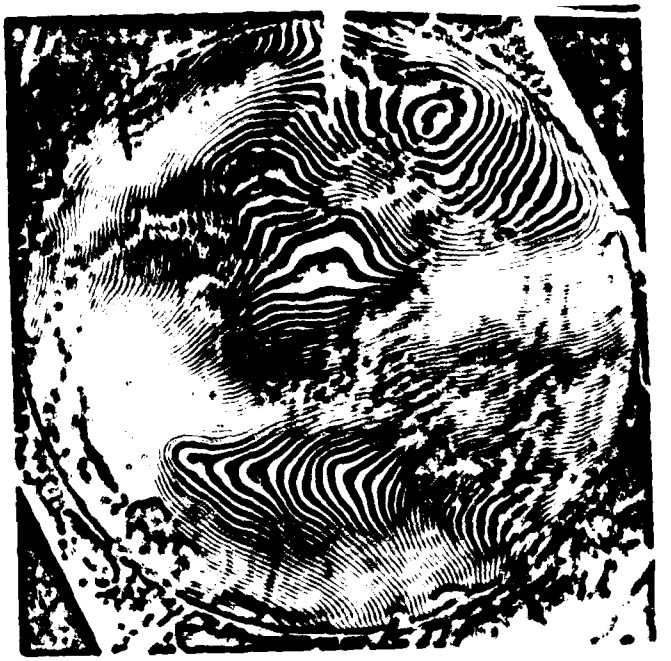

(A)

(B)

21. (a) Moiré fringe pattern between [illegible] points indicated as A and B in Figure 5. (b) Moiré fringe pattern between photographs taken at points indicated as [illegible] in Figure 5.

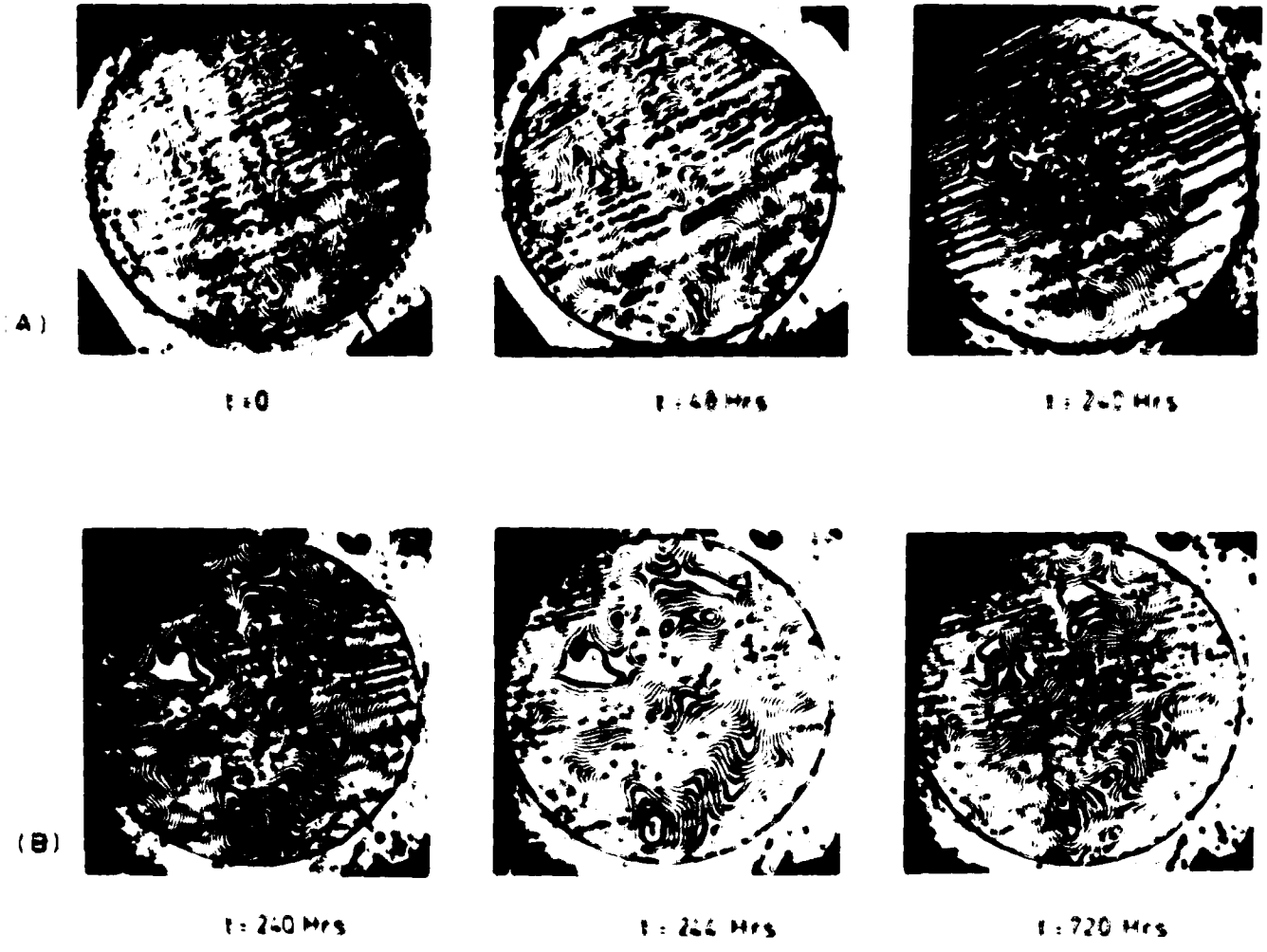

11. Sequence of interference photographs for a second [illegible] specimen, (A) immersed in distilled water at 62C and (B) exposed to dry air at 62C. The arrow indicates the onset of debonding

1/2 hr

2 hrs

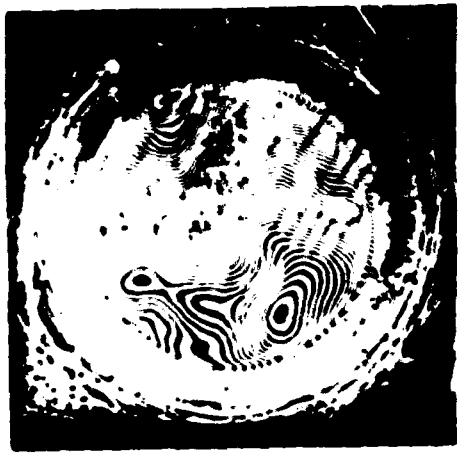

6 hrs

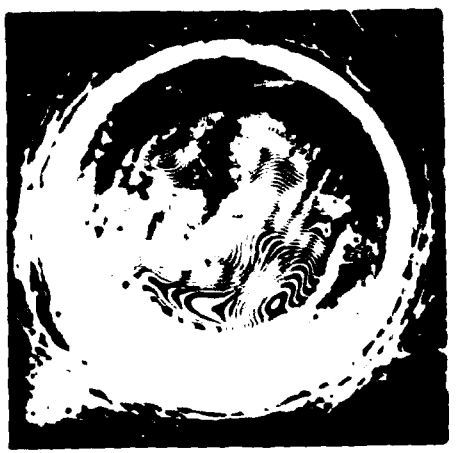

23 hrs

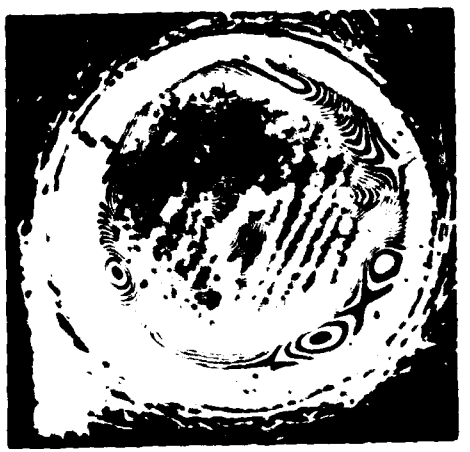

76 hrs

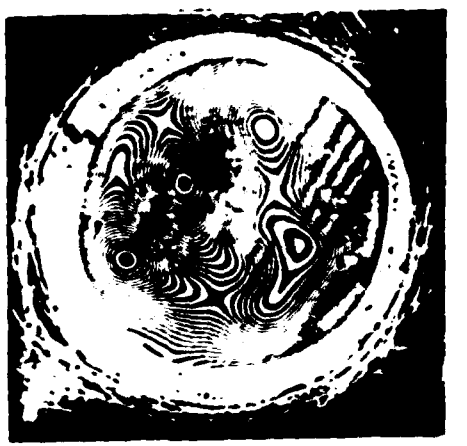

192 hrs

23. Sequence of interference photographs for a EY 1000 specimen immersed

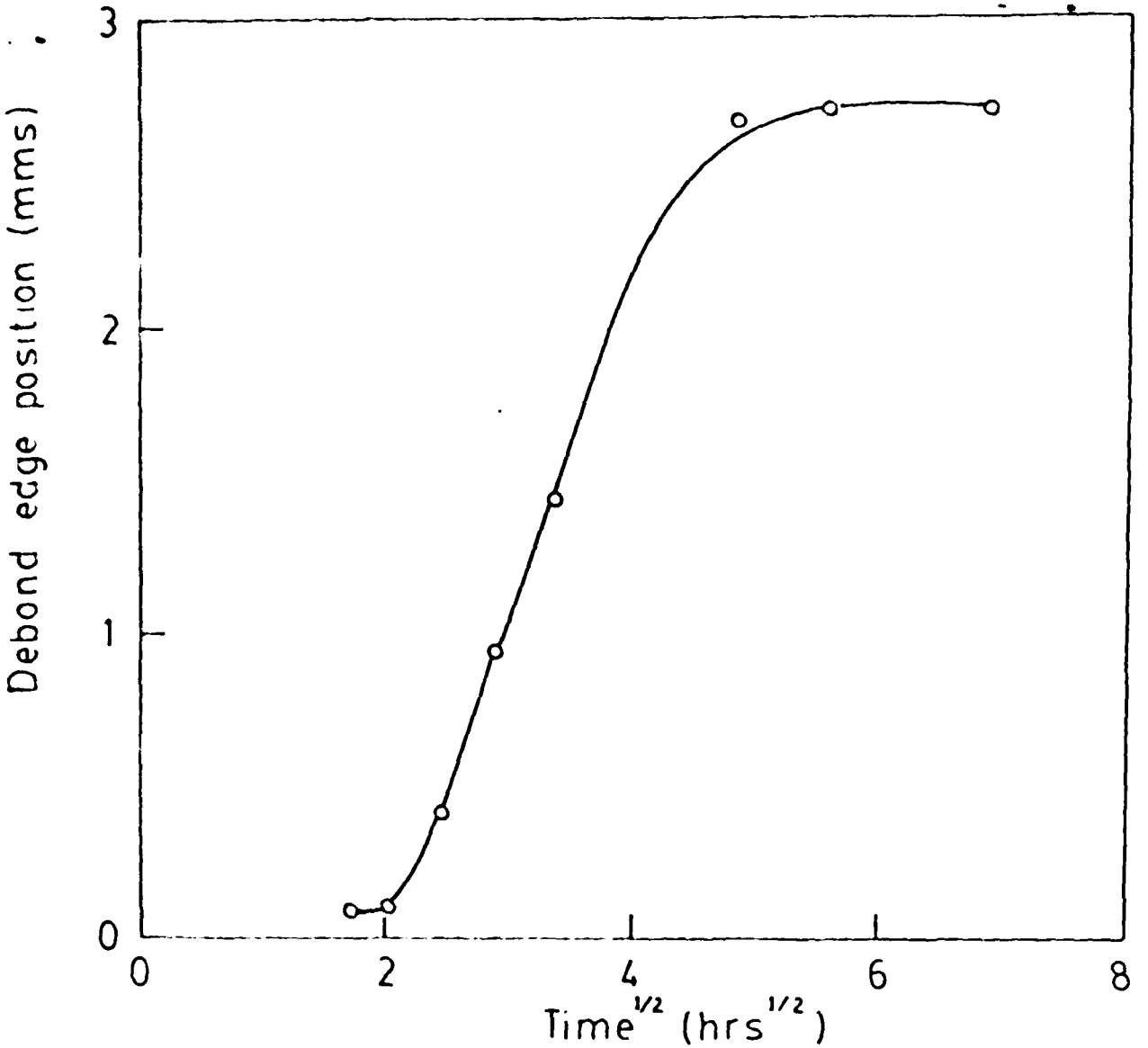

24. Graph of the position of the debonding edge at the cover slip/adhesive interface plotted as a function of time$^{1/2}$ for the specimen shown in Figure 23

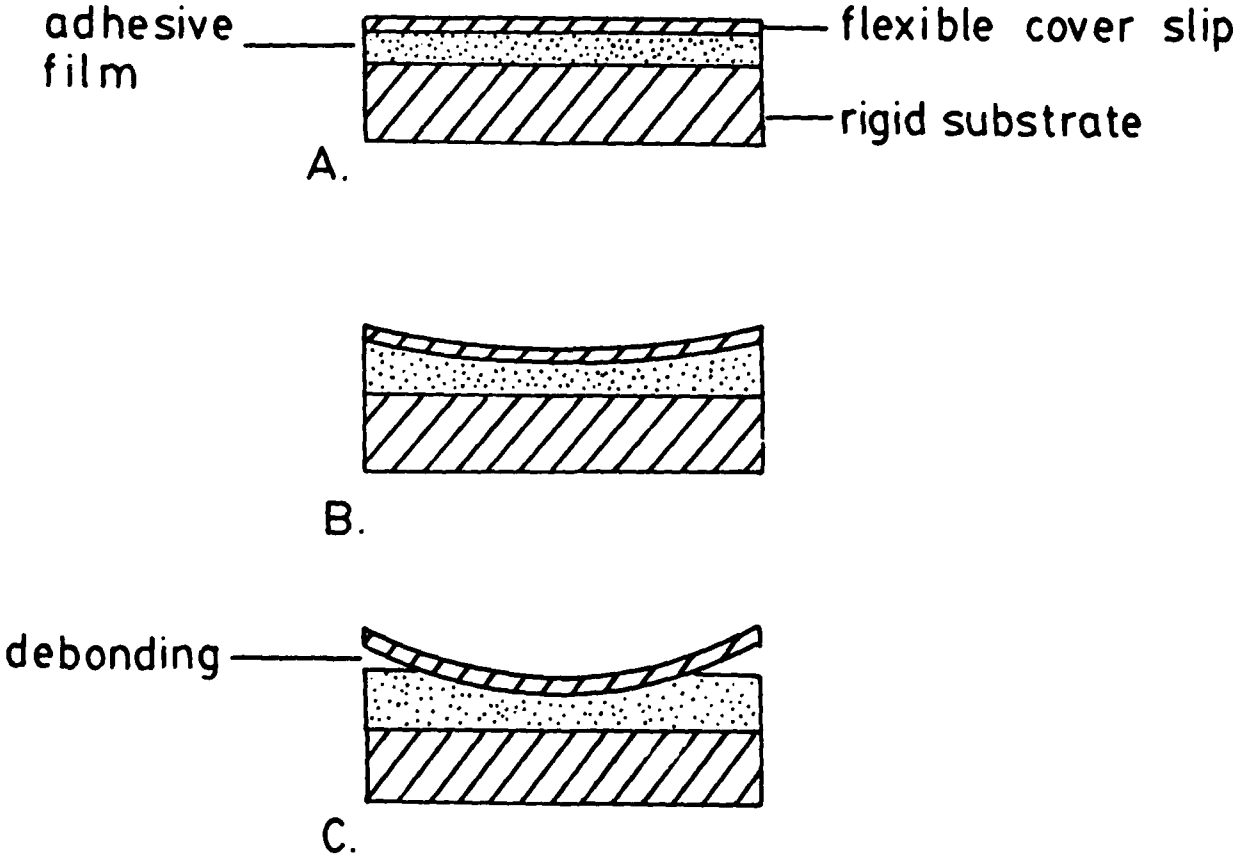

25. Schematic diagram to illustrate the changing geometry of the cover slip during swelling of the adhesive in a joint exposed to an aqueous environment. Debonding follows saturation of swelling at the rim of the joint

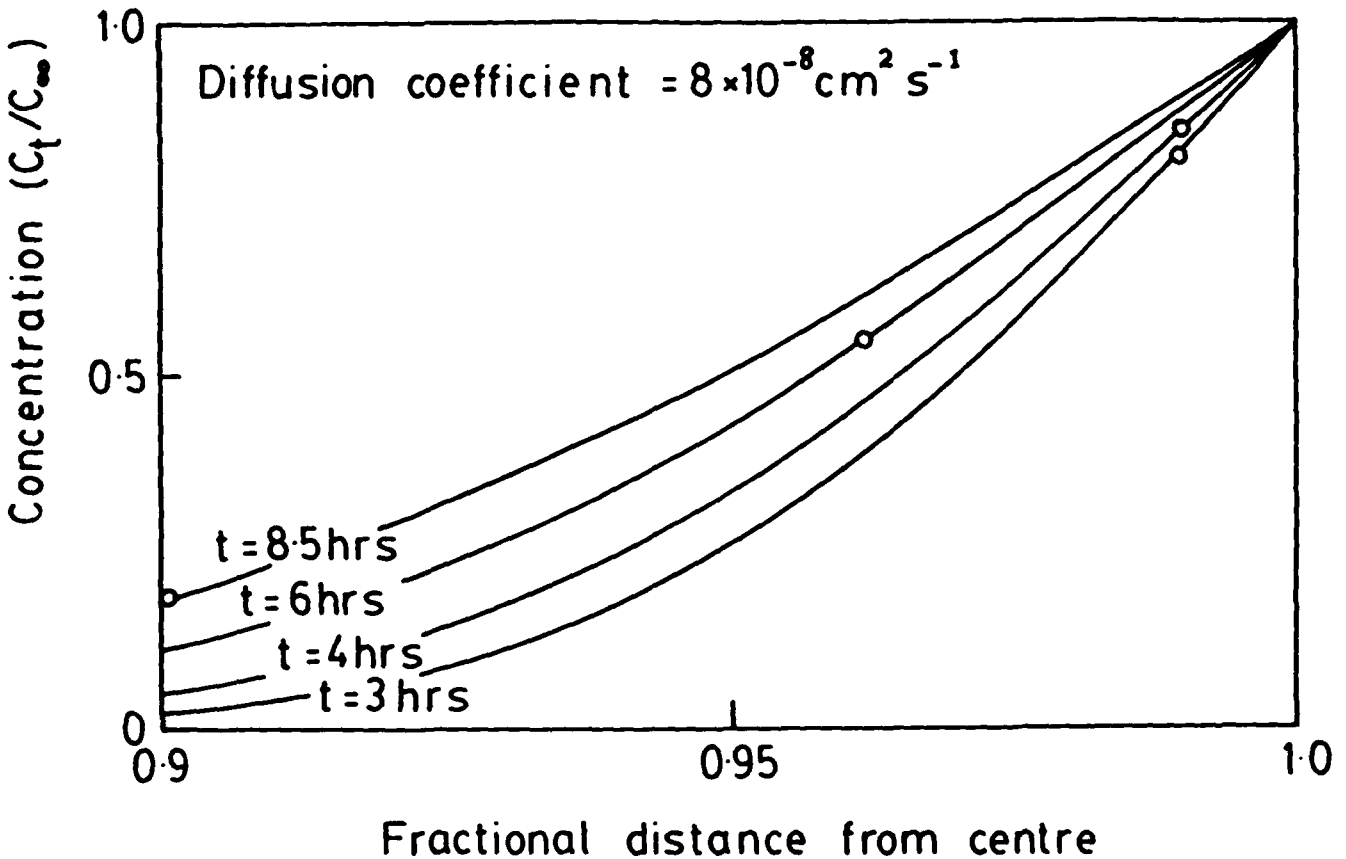

26. Graph of the predicted water concentration (C_t/C_∞) as a function of fractional distance from the centre of the specimen. O, points representing te critical concentrations for positions corresponding to the debonding edge shown in Figure 25. After Kinloch[9].


DATE
ILME
8